Comparative Study of Predictive-Fixed Switching Techniques for a Cascaded H-Bridge Two level STATCOM

Alfredo Renault[1], Magno Ayala[1], Leonardo Comparatore[1], Julio Pacher[1] and Raul Gregor[1]
[1]*Laboratory of Power and Control Systems, Facultad de Ingeniería, Universidad Nacional de Asunción, Paraguay*
E-mail: {arenault, mayala, lcomparatore, jpacher & rgregor }@ing.una.py

***Abstract*—Finite state model predictive control methods are distinguished by a variable switching frequency which causes large current ripples at low sampling frequency. This paper presents a comparative study of two enhanced predictive current control techniques with fixed switching frequency applied to the three-wire cascaded H-bridge two level converter for active power filter applications. Simulation results are developed to demonstrate the performance of the two proposed predictive control techniques in terms of mean square error, root mean square and total harmonic distortion as figures of merit, thus concluding the advantages and limitations of each technique at transient and steady states.**

***Index Terms*—Active power filter, cascaded H-bridge power converter, finite state model predictive control, fixed switching frequency.**

NOMENCLATURE

APF	Active power filter.
CHB	Cascade H-bridge.
FCS-MPC	Finite-control-set model predictive control.
MPC	Model predictive control.
MSE	Mean square error.
PCC	Point of common coupling.
RMS	Root mean square.
STATCOM	Static compensator.
THD	Total harmonic distortion.
VSI	Voltage source inverter.
C_{dc}	DC-link capacitor.
g_a, g_b, g_c	FCS-MPC cost functions.
i_s^a, i_s^b, i_s^c	Power grid phase currents.
i_L^a, i_L^b, i_L^c	Load phase currents.
i_c^a, i_c^b, i_c^c	STATCOM phase currents.
$\hat{i}_c^a$, $\hat{i}_c^b$, $\hat{i}_c^c$	STATCOM phase current predictions.
$i_{c\alpha}$, $i_{c\beta}$	STATCOM currents in the $\alpha-\beta$ subspace.
i_c^{a*}, i_c^{b*}, i_c^{c*}	STATCOM phase current references.
v_c^a, v_c^b, v_c^c	STATCOM phase voltages.
n_c	Number of cells.
P_c^*	Instantaneous active power reference.
P_L	Instantaneous active load power.
Q_c^*	Instantaneous reactive power reference.
Q_L	Instantaneous reactive load power.
$\mathbf{T}$	Clarke's transformation matrix.
T_s	Sampling time.
V_{dc}	DC-link voltage.

I. INTRODUCTION

Due to the increase of non-linear and reactive loads in recent years, there was an increase of the harmonics amplitudes in the electrical distribution network and the consumption of reactive power [1]. To mitigate this problem, one of the main current solutions to this problem is the use of APF which is responsible for compensating the harmonics of the electrical network and reactive power [2]. APFs are based on power converters such as VSI [3], NPC [4] and H-Bridges [5], [6]. APFs based on H-bridge converters with SiC-MOSFET switching devices have several advantages, such as the possibility of scalability, modular structure and higher switching frequency [7]. Due to these advantages, they have been object of study and are now considered a very competitive topology in the new generation APF based on power converters and can be applied to the electrical distribution power grid [8]. On the other hand, nowadays, MPC is considered a valid alternative to classic controllers and is very used in different applications, due to the improvement of the micro-processor technology, which allows a higher computation speed where the MPC control offers several advantages such as speed response and easy inclusion of no linearities, which makes it suitable for multivariable systems [9]. There are several studies of the MPC control applied to power converters and complex systems such as PFs [10], [11], multiphase machines [12]–[15], matrix converters [16], [17], among others. However, some of the main disadvantages presented by MPC control are stability, steady state error and variable switching frequency which causes high peaks current ripple in the converter output and power losses [18]–[21].

This paper proposes a comparative study of modulated MPC control methods applied to the three-phase APF based on two-level H-bridge converters, obtaining a fixed switching frequency. The comparison is made in terms of MSE current tracking, power ripple RMS and the grid current THD as figures of merit. This paper is organized as follows: Section II describes the three-phase H-bridge APF topology. Section III and Section IV expose the modulated MPC strategies to compare. Section V illustrates the performance of the proposed techniques considering the simulation results. Finally, the conclusion is presented in Section VI.

978-1-5386-2910-9/18/$31.00

II. System description

The system under study consists in a two-level three-phase CHB STATCOM depicts in Fig. 1. Notice that each cell of the CHB have an independent DC-link and four switching devices, typically IGBTs or SiC MOSFETs. Then, four firing signals, represented by S_{fxy} are used to control each cell, being f the phase ($f = a$, b or c), x the cell number in each phase and y the switching device in each cell ($y = 1$, 2, 3 or 4). Table I shows the allowed combination of the firing signal taking phase "a" as example. Similar analysis can be easily extended to other phases considering allowed combinations and avoid short circuit in the DC-link of each cell.

Then, the dynamic of the system's model can be obtained by using Kirchhoff's circuit laws. The imbalance in the three-phase voltage sources as well as the capacitance and DC-link voltages are beyond the scope of this paper, and only balance conditions are considered. Notice that the CHB converter-based STATCOM is connected at the PCC. Next, by applying Kirchhoff's laws for the ac side of the STATCOM, the following equations are obtained:

$$\begin{aligned}\frac{\mathrm{d}i_c^a}{\mathrm{d}t} &= 1/L_f\left(v_s^a - R_f\, i_c^a - n_c\, Sa_{ij}\, v_{\mathrm{dc}}^a\right)\\ \frac{\mathrm{d}i_c^b}{\mathrm{d}t} &= 1/L_f\left(v_s^b - R_f\, i_c^b - n_c\, Sb_{ij}\, v_{\mathrm{dc}}^b\right)\\ \frac{\mathrm{d}i_c^c}{\mathrm{d}t} &= 1/L_f\left(v_s^c - R_f\, i_c^c - n_c\, Sc_{ij}\, v_{\mathrm{dc}}^c\right)\end{aligned} \tag{1}$$

$$\begin{aligned}\frac{\mathrm{d}v_{\mathrm{dc}}^a}{\mathrm{d}t} &= \frac{Sa_{ij}}{C_{\mathrm{dc}}} i_c^a - \frac{v_{\mathrm{dc}}^a}{R_{\mathrm{dc}}\, C_{\mathrm{dc}}}\\ \frac{\mathrm{d}v_{\mathrm{dc}}^b}{\mathrm{d}t} &= \frac{Sb_{ij}}{C_{\mathrm{dc}}} i_c^b - \frac{v_{\mathrm{dc}}^b}{R_{\mathrm{dc}}\, C_{\mathrm{dc}}}\\ \frac{\mathrm{d}v_{\mathrm{dc}}^c}{\mathrm{d}t} &= \frac{Sc_{ij}}{C_{\mathrm{dc}}} i_c^c - \frac{v_{\mathrm{dc}}^c}{R_{\mathrm{dc}}\, C_{\mathrm{dc}}}\end{aligned} \tag{2}$$

being, R_{dc} a resistor connected in parallel to C_{dc} that concentrates the overall losses in the DC side and R_f is the parasitic (series) resistance of the inductor L_f.

A. Classic FCS-MPC strategy

In classic FCS-MPCs the mathematical model is used to predict the future behavior of the system. In this case, the differential equations of the system in the AC side is represented by the following equations:

$$\begin{aligned}\frac{\mathrm{d}i_c^a}{\mathrm{d}t} &= 1/L_f\left(v_s^a - v_c^a - R_f\, i_c^a\right)\\ \frac{\mathrm{d}i_c^b}{\mathrm{d}t} &= 1/L_f\left(v_s^b - v_c^b - R_f\, i_c^b\right)\\ \frac{\mathrm{d}i_c^c}{\mathrm{d}t} &= 1/L_f\left(v_s^c - v_c^c - R_f\, i_c^c\right).\end{aligned} \tag{3}$$

Then, the predictive model can be obtained by using a forward-Euler discretization method due to its simplicity, however other discretization methods can be used such as the matrix factorization introduced by Cayley-Hamilton. The discrete-time model is given by:

TABLE I
Possible Combinations of activation signals

Sa_{11}	Sa_{13}	Sa_{12}	Sa_{14}	v_c^a
1	0	0	1	$+v_{\mathrm{dc}}$
1	1	0	0	0
0	0	1	1	0
0	1	1	0	$-v_{\mathrm{dc}}$

$$\begin{aligned}\hat{i}_{c[k+1|k]}^a &= A_1\, i_{c[k]}^b + T_s/L_f\,\left(v_{s[k]}^a - v_{c[k]}^a\right)\\ \hat{i}_{c[k+1|k]}^b &= A_1\, i_{c[k]}^b + T_s/L_f\,\left(v_{s[k]}^b - v_{c[k]}^b\right)\\ \hat{i}_{c[k+1|k]}^c &= A_1\, i_{c[k]}^c + T_s/L_f\,\left(v_{s[k]}^c - v_{c[k]}^c\right)\end{aligned} \tag{4}$$

being $A_1 = \left(1 - \frac{R_f T_s}{L_f}\right)$.

In the case of a current control, the typical cost function is defined as the difference between reference currents and the predicted currents:

$$\begin{aligned} g_a &= \| \, i_c^{a^*} - \hat{i}_{c[k+1]}^a \, \|^2\\ g_b &= \| \, i_c^{b^*} - \hat{i}_{c[k+1]}^b \, \|^2\\ g_c &= \| \, i_c^{c^*} - \hat{i}_{c[k+1]}^c \, \|^2 .\end{aligned} \tag{5}$$

Next, the cost function is evaluated for each switching states and for each phase. The switching state that minimizes the cost function is applied to each phase of the CHB STATCOM during the next sampling time causing a variable switching frequency for each phase.

B. Current reference generation

For the evaluation of the cost function in (5) is necessary the current references. For simplicity, the phase currents and voltages are translated to the $\alpha-\beta$ subspace by using Clarke's transformation matrix:

$$\mathbf{T} = \sqrt{\frac{2}{3}} \begin{bmatrix} 1 & -\frac{1}{2} & -\frac{1}{2} \\ 0 & \frac{\sqrt{3}}{2} & -\frac{\sqrt{3}}{2} \\ \frac{1}{\sqrt{2}} & \frac{1}{\sqrt{2}} & \frac{1}{\sqrt{2}} \end{bmatrix}. \tag{6}$$

Then, the current references in $\alpha - \beta$ subspace in function of active and reactive power are:

$$\begin{bmatrix} i_{c\alpha}^* \\ i_{c\beta}^* \end{bmatrix} = \frac{1}{(v_{s\alpha})^2 + (v_{s\beta})^2} \begin{bmatrix} v_{s\alpha} & v_{s\beta} \\ v_{s\beta} & -v_{s\alpha} \end{bmatrix} \begin{bmatrix} P_c^* \\ Q_c^* \end{bmatrix}. \tag{7}$$

In order to have a unit power factor on the grid side $P_c^* = 0$, then the STATCOM does not absorb active power and the instantaneous reactive power reference can be written as:

$$Q_c^* = -Q_L = v_{s\alpha}\, i_{L\beta} - v_{s\beta}\, i_{L\alpha} \tag{8}$$

where Q_L is compensated by the CHB STATCOM system. The STATCOM phase currents references used in the optimization process are:

$$\begin{bmatrix} i_c^{a^*} \\ i_c^{b^*} \\ i_c^{c^*} \end{bmatrix} = \mathbf{T}^{-1} \begin{bmatrix} i_{c\alpha}^* \\ i_{c\beta}^* \\ 0 \end{bmatrix}. \tag{9}$$

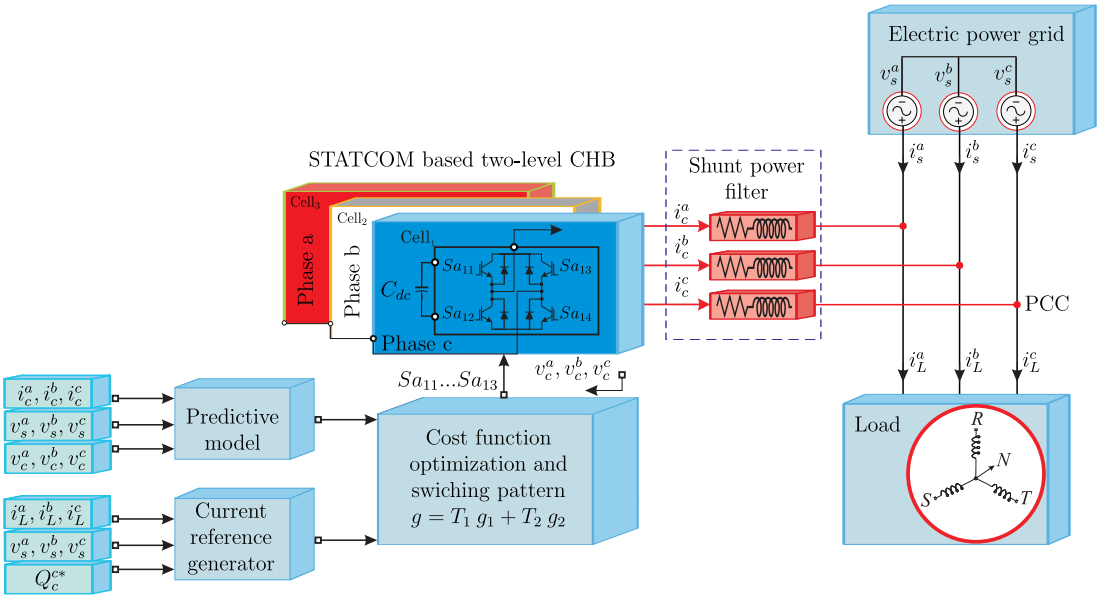

Fig. 1. Control scheme of the proposed modulated FCS-MPC.

III. Modulated FCS-MPC method (M2PC)

The general scheme of the proposed modulated FCS-MPC is shown in Fig. 1. This M2PC uses two active vectors and two null vectors in conjunction with a switching pattern exposed in Fig. 2, therefore it can be seen as space vector modulation. This method first follows the same procedure as classic FCS-MPC technique explained in the previous section. After the evaluation of the current predictions (4), cost function (5) and currents references (9), the optimum voltage vector is obtained through the combination of the two active vectors and the two null vectors [22], [23]. Then, the proposed method evaluates the cost function, namely g_0, g_1 and g_2, of each voltage vector (active and null) to estimate the duty cycles for each vector and these are computed by solving the following equations:

$$T_0 = \frac{K}{g_0} \tag{10}$$

$$T_1 = \frac{K}{g_1} \tag{11}$$

$$T_2 = \frac{K}{g_2} \tag{12}$$

$$T_0 + T_1 + T_2 = T_s \tag{13}$$

By solving the system of (13), it is possible to obtain the expression for K and the expressions for the duty cycles:

$$T_1 = \frac{g_0 g_2}{g_0 g_1 + g_0 g_2 + g_1 g_2} \tag{14}$$

$$T_2 = \frac{g_0 g_1}{g_0 g_1 + g_0 g_2 + g_1 g_2} \tag{15}$$

$$T_0 = 1 - T_1 - T_2 \tag{16}$$

According to these expressions, the new cost function, which is evaluated at every sampling time for each phase, is defined:

$$g = T_1\, g_1 + T_2\, g_2 \tag{17}$$

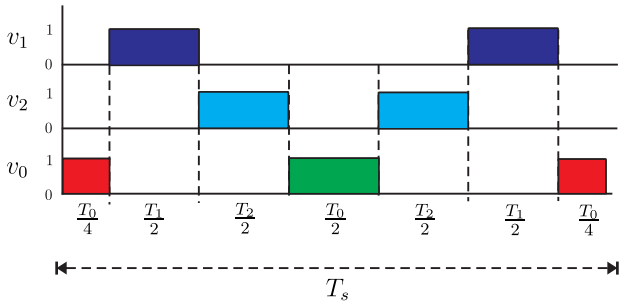

Fig. 2. Switching pattern of the proposed modulated FCS-MPC.

IV. Modulated FCS-MPC technique (PWM)

The FCS-MPC technique selects an optimal vector from the minimization of the cost function in (5). Instead of applying the chosen voltage vector to the CHB during the whole switching period, which is the procedure in conventional FCS-MPC schemes, then a PWM method is added to the FCS-MPC output to obtain a fixed-switching frequency. The duty cycles depend on the generated voltage level in the CHB where, according to Table I, there are three voltage levels ($+v_{dc}$, $-v_{dc}$ and 0). By using conditions it is possible to estimate the duty cycle for a switching device which obtains a similar voltage level as shown in Table II. The duty cycles generate a fixed switching frequency for every switching device improving the performance over classic FCS-MPC.

TABLE II
Possible duty cycles of activation signals

Sa_{11}	Sa_{13}	v_c^a
0.95	0.05	$+v_{dc}$
0.5	0.5	0
0.05	0.95	$-v_{dc}$

V. Simulation Results

This section exposes the performance of the proposed modulated FCS-MPC techniques by using a MATLAB/Simulink simulation tool. A numerical integration based on Ode1 Euler was used for the calculation of fixed step in the time domain with a relative tolerance of 1 μs and with $T_s = 50$ μs. The grid frequency and voltage are set 50 Hz and 310.2 V, respectively. Other electrical parameters are $v_{\text{dc}} = 400$ V, $R_f = 0.09$ Ω, $L_f = 9$ mH, $R_L = 23.2$ Ω and $L_L = 55$ mH.

The two-level CHB STATCOM is connected at $t = 0.02$ s, compensating the reactive power of the grid showing a fast dynamic response for both modulation techniques exposed in Fig. 3. In this test the active and reactive power are set to $Q_L = 3\,000$ VAR and $P_L = 4\,000$ W, respectively. The mean value of Q_s for M2PC and PWM are 1.978 and 2.853 VAR respectively, compensating a 99.93 and 99.90 % of the load reactive power. On the other hand, the RMS of P_s and Q_s ripple for M2PC are 87.13 W, 59.94 VAR and for PWM are 164.18 W, 175.38 VAR, respectively. At last, by considering the mean value of P_s for both modulation techniques, the power efficiency of the CHB STATCOM is about 99.30 and 98.86 % for M2PC and PWM, respectively.

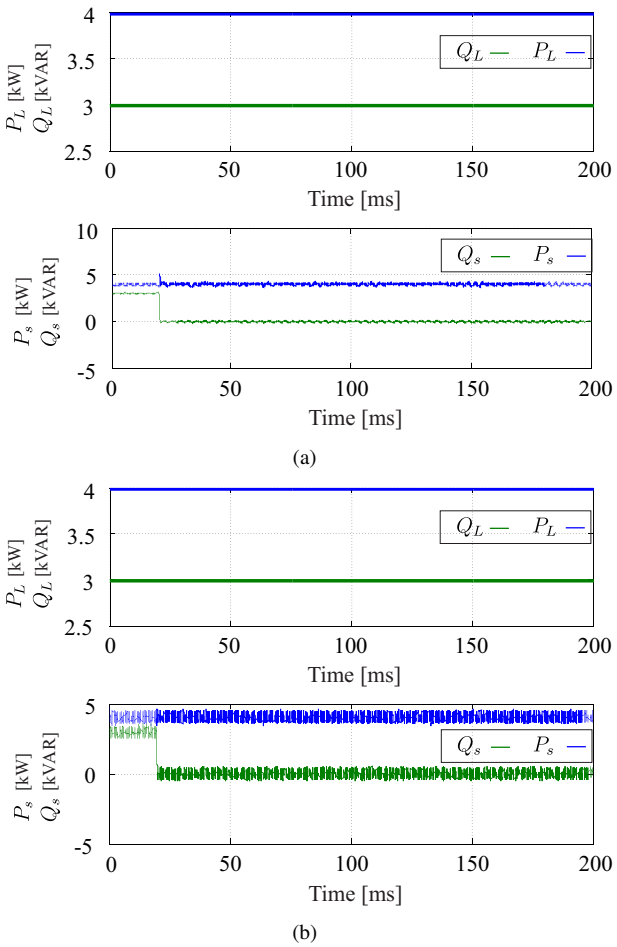

Fig. 3. Two-level CHB STATCOM response for M2PC, active and reactive power compensation, (above) in the load and (bottom) in the power grid: (a) M2PC; (b) PWM.

The current injected by the two-level CHB STATCOM presents an excellent and fast tracking of its reference as shown shown Fig. 4, for phase a. In order to quantify the performance tracking of the injected current, the MSE of the measured current and the reference is considered. The obtained values for both techniques are 166.5 and 373.4 mA for M2PC and PWM, respectively.

Then, Fig. 5 and Fig. 6 show the two-level CHB STATCOM voltage output, which show a two level pattern plus the null voltage level, and the harmonic spectrum for the grid current, where the THD for the grid current are 2.57 and 5.89 % for M2PC and PWM, respectively. It can also be seen in the harmonic spectrum the dominant harmonic switching frequency of 20 kHz and its multiples which is the fixed switching frequency of the system.

Similar results have been obtained for phases b and c and have not been included for the sake of conciseness.

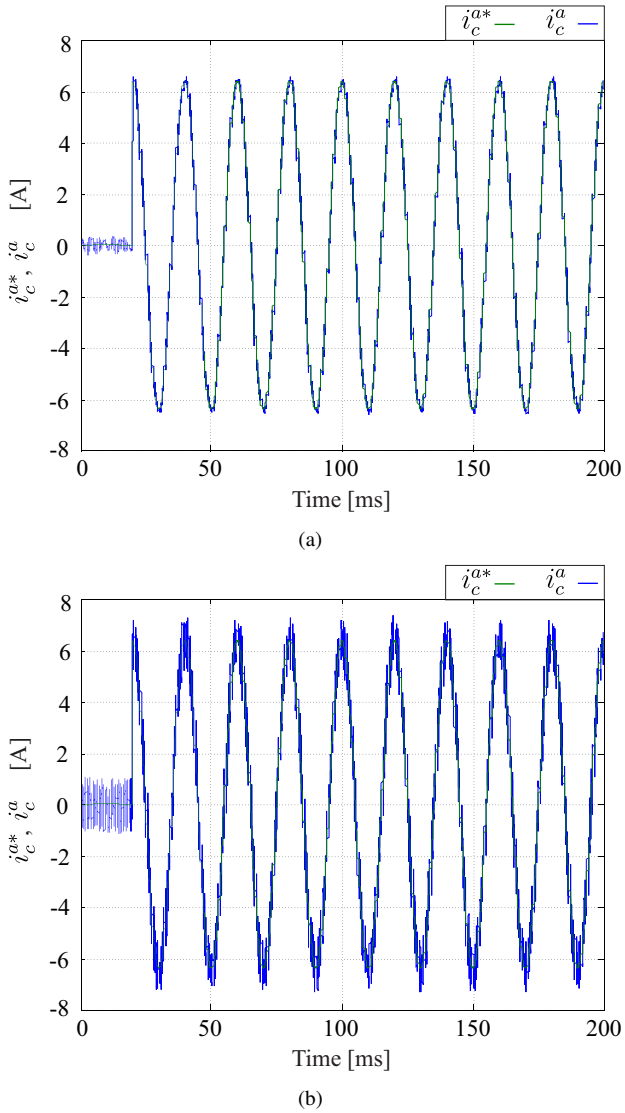

Fig. 4. Two-level CHB STATCOM response for M2PC, active and reactive power compensation, (above) in the load and (bottom) in the power grid: (a) M2PC; (b) PWM.

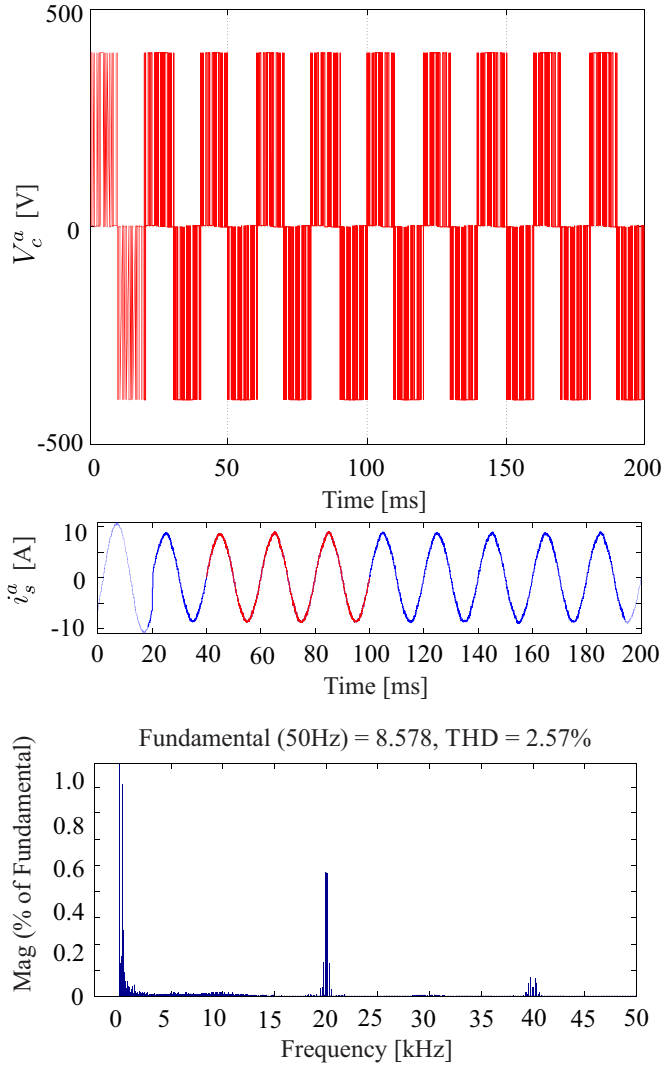

Fig. 5. (above) APF voltage, (middle) the grid current evolution at PCC, (bottom) the THD of the grid current for M2PC.

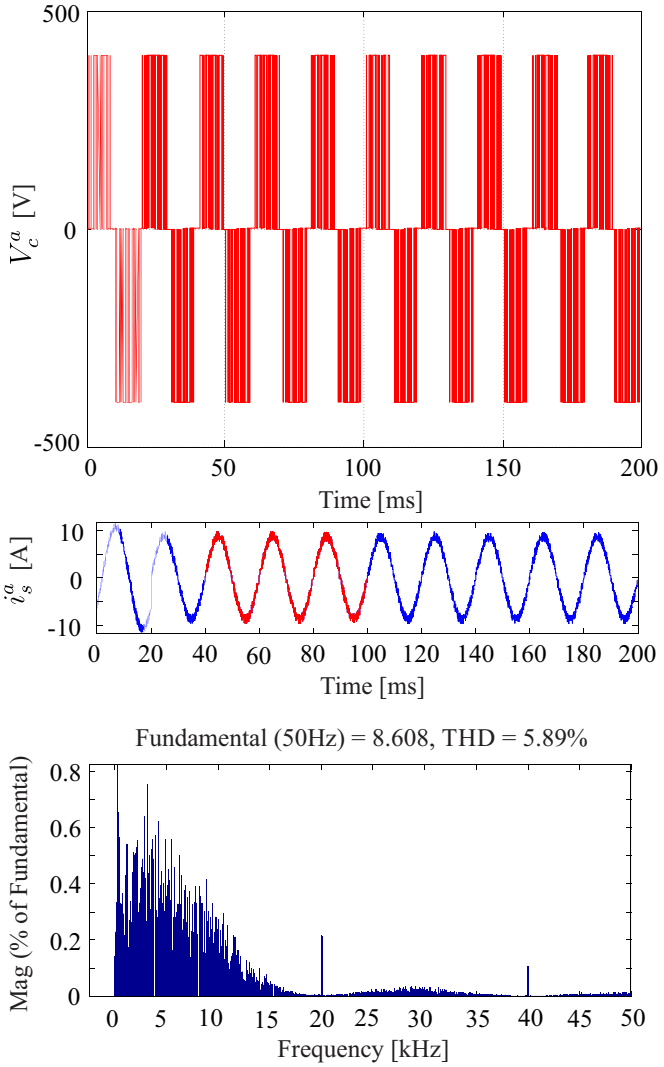

Fig. 6. (above) APF voltage, (middle) the grid current evolution at PCC, (bottom) the THD of the grid current for PWM.

VI. Conclusion

This paper has presented a comparative study between two FCS-MPC with fixed switching frequency. It has been shown that both techniques, M2PC and PWM, are powerful alternatives to current controller of a two-level three-phase CHB STATCOM. While, in transient conditions, both techniques have very similar dynamics, in steady states, M2PC techniques shows a better performance over PWM in every considered parameter, such as the current grid THD, the injection current MSE and the RMS power ripple and power efficiency. The only drawback presented for M2PC compared to PWM is the computational cost, which it is assumed to be higher due to the fact that M2PC needs more calculation process to obtain the optimal duty cycles. Still both techniques are considered to be valuable alternatives to classic FCS-MPC with variable switching frequency. From the point of view of the charge of the H-bridge capacitors, further research will be necessary to find an optimal switching pattern.

Acknowledgment

The authors wish to thank the financial support from the Paraguayan Science and Technology National Council (CONACYT) through project 14-INV-96.

References

[1] G. Son, H.-J. Kim, and B.-H. Cho, "Improved modulated carrier control with on-time doubler for a single-phase shunt active power filter," *IEEE Trans. on Power Electronics*, vol. 33, no. 2, pp. 1715–1723, 2018.

[2] R. Rabbeni, L. Tarisciotti, A. Gaeta, A. Formentini, P. Zanchetta, M. Pucci, M. Degano, and M. Rivera, "Finite states modulated model predictive control for active power filtering systems," in *Proc. ECCE*. IEEE, 2015, pp. 1556–1562.

[3] V. Gali, N. Gupta, and R. Gupta, "Distortion free improved reference current generation algorithm for interleaved inverter based shunt APF," in *Proc. APPEEC*. IEEE, 2017, pp. 1–6.

[4] M. Kashif, M. Hossain, Y. R. Kafle, and M. S. Rahman, "A comparative study of two current-control techniques applied to a three-phase three-level active power filter," in *Proc. INTELEC*. IEEE, 2017, pp. 357–362.

[5] M. Mane and M. K. Namboothiripad, "Pwm based sliding mode controller for shunt active power filter," in *Proc. ICNTE*. IEEE, 2017, pp. 1–6.

[6] R. Gregor, L. Comparatore, A. Renault, J. Rodas, J. Pacher, S. Toledo, and M. Rivera, "A novel predictive-fixed switching frequency technique for a cascade H-bridge multilevel STATCOM," in *Proc. IECON*. IEEE, 2016, pp. 3672–3677.

[7] V. Tummakuri, B. Das, P. R. Kasari, and A. Chakraborti, "Grid connected five level cascaded H bridge inverter as shunt active power filter," in *Proc. NPEC*. IEEE, 2017, pp. 60–65.

[8] J. Pacher, J. Rodas, R. Gregor, M. Rivera, A. Renault, and L. Comparatore, "Efficiency analysis of a modular H-bridge based on SiC MOSFET," *International Journal of Electronics Letters*, no. just-accepted, 2018.

[9] S. Bifaretti, S. Pipolo, A. Lidozzi, L. Solero, L. Tarisciotti, and P. Zanchetta, "Modulated model predictive control for active split DC-bus 4-leg power supply," in *Proc. ECCE*. IEEE, 2017, pp. 4622–4627.

[10] A. Renault, M. Riveray, L. Comparatore, J. Pacher, J. Rodas, and R. Gregor, "Model predictive current control with neutral current elimination for H-bridge two-level active power filters," in *Proc. ETCM*. IEEE, 2016, pp. 1–5.

[11] L. Comparatore, R. Gregor, J. Rodas, J. Pacher, A. Renault, and M. Rivera, "Model based predictive current control for a three-phase cascade H-bridge multilevel STATCOM operating at fixed switching frequency," in *Proc. PEDG*. IEEE, 2017, pp. 1–6.

[12] J. Rodas, F. Barrero, M. R. Arahal, C. Martin, and R. Gregor, "On-line estimation of rotor variables in predictive current controllers: A case study using five-phase induction machines," *IEEE Trans. Ind. Electron.*, vol. 63, no. 9, pp. 5348–5356, 2016.

[13] J. Rodas, C. Martin, M. R. Arahal, F. Barrero, and R. Gregor, "Influence of covariance-based ALS methods in the performance of predictive controllers with rotor current estimation," *IEEE Trans. Ind. Electron.*, vol. 64, no. 4, pp. 2602–2607, 2017.

[14] M. Ayala, J. Rodas, R. Gregor, J. Doval-Gandoy, O. Gonzalez, M. Saad, and M. Rivera, "Comparative study of predictive control strategies at fixed switching frequency for an asymmetrical six-phase induction motor drive," in *Proc. IEMDC*, pp. 1–8, 2017.

[15] M. Ayala, O. Gonzalez, J. Rodas, R. Gregor, and J. Doval-Gandoy, "A speed-sensorless predictive current control of multiphase induction machines using a Kalman filter for rotor current estimator," in *Proc. ESARS-ITEC*. IEEE, 2016, pp. 1–6.

[16] E. Maqueda, S. Toledo, R. Gregor, D. Caballero, F. Gavilán, J. Rodas, M. Rivera, and P. Wheeler, "An assessment of predictive current control applied to the direct matrix converter based on SiC-MOSFET bidirectional switches," in *Proc. SPEC*. IEEE, 2017, pp. 1–6.

[17] Z. Di, M. Rivera, H. Dan, L. Tarisciotti, K. Zhang, D. Xu, and P. Wheeler, "Modulated model predictive current control of an indirect matrix converter with active damping," 2017.

[18] F. Gavilan, D. Caballero, S. Toledo, E. Maqueda, R. Gregor, J. Rodas, M. Rivera, and I. Araujo-Vargas, "Predictive power control strategy for a grid-connected 2L-VSI with fixed switching frequency," in *Proc. ROPEC*. IEEE, 2016, pp. 1–6.

[19] A. Renault, M. Rivera, J. Rodas, L. Comparatore, J. Pacher, and R. Gregor, "Modulated model predictive current control for H-bridge two-level single phase active power filters STATCOM," in *Proc. ICIEA*. IEEE, 2017, pp. 355–359.

[20] L. Tarisciotti, A. Formentini, A. Gaeta, M. Degano, P. Zanchetta, R. Rabbeni, and M. Pucci, "Model predictive control for shunt active filters with fixed switching frequency," *IEEE Trans. on Industry Applications*, vol. 53, no. 1, pp. 296–304, 2017.

[21] L. Alhafadhi, J. Asumadu, and A. Alsafi, "Total harmonics distortion reduction using adaptive, weiner, and Kalman filters," in *Proc. CCWC*. IEEE, 2017, pp. 1–8.

[22] S. Toledo, M. Rivera, J. Muñoz, R. Peña, J. Riveros, and R. Gregor, "Fixed switching frequency predictive control for a multi-drive indirect matrix converter system," in *Proc. SPEC*, pp. 1–6, 2017.

[23] M. Rivera, S. Toledo, C. Baier, L. Tarisciotti, P. Wheeler, and S. Verne, "Indirect predictive control techniques for a matrix converter operating at fixed switching frequency," in *Proc. PRECEDE*, pp. 13–18, 2017.